

## Spacecraft formation flying system design and controls for four nanosats mission

Youngbum Song<sup>a</sup>, Sang-Young Park<sup>a,\*</sup>, Sangwon Lee<sup>a</sup>, Pureum Kim<sup>a</sup>, Eunji Lee<sup>a</sup>, Jaejin Lee<sup>b</sup>

<sup>a</sup> Department of Astronomy, Yonsei University, 50 Yonsei-ro Seodaemun-gu, Seoul, 03722, Republic of Korea

<sup>b</sup> Space Science Division, Korea Astronomy and Space Science Institute, 776 Daedeok-daero Yuseong-gu, Daejeon, 34055, Republic of Korea

### ARTICLE INFO

#### Keywords:

drift Recovery  
Formation flying  
Ground-based orbit control  
Orbit control scenario  
Orbit control simulation  
SNIPE

### ABSTRACT

Small-scale magNetosphere and Ionosphere Plasma Experiment (SNIPE) mission is aimed to observe a small-scale structure of the physical phenomena in a near-Earth environment. SNIPE mission comprises four 6U size nanosats that perform formation flying to meet the scientific objectives of the mission. In this study, we designed a formation flying system and validated it using numerical simulations to collect temporal and spatial differences of the physical phenomena for the SNIPE mission. The requirements for spacecraft formation flying are to pass the same point at different times and be located at different longitude points on the same latitude. Two types of formations which are an along-track formation for temporal observations and a cross-track formation for spatial observations are devised. The size of the formation decreases during the along-track formation phase and increases during the cross-track formation phase. Four types of orbit control were introduced to implement these formations and adjust the relative distances between the nanosats. Changing the shape and size of the formation exploits the effects of perturbations through orbit controls. The simulations were considered with several constraints to replicate the intended environments. The simulations also reflect the time differences between the orbit determination epoch and orbit control epoch, conditions in attitude control of nanosats, limitations of orbit control operation time to secure power stability, and errors in the thrust module. The numerical simulations demonstrated that each nanosat satisfied the mission requirements in a  $\Delta V$  budget of 50 m/s. These results verified that the designed formation flying system meets the scientific objectives of SNIPE mission by changing the shape and size of the formation.

### 1. Introduction

Small-scale magNetosphere and Ionosphere Plasma Experiment (SNIPE) mission is an Earth science mission developed by Korea Astronomy and Space Science Institute, Korea Aerospace Research Institute, and Yonsei University. The mission aims to study the geomagnetic field by observing physical phenomena that occur in the near-Earth environment. The target phenomena by the SNIPE mission includes electron microbursts, plasma trough, electron density and temperature, length of coherence for bubbles/blobs, and electromagnetic ion cyclotron (EMIC) waves as shown in Fig. 1 [1,2]. In particular, EMIC waves should be detected at the equator and near the aurora region at latitudes over 70°. Various small-scale structures from 10 km to thousands of kilometers are observed by the mission to study the physical phenomena. The SNIPE mission comprises four 6U Nanosats that perform the formation flying to observe small scale structure of the physical

phenomena. 1U (100 × 100 × 100 mm) is a standard that represents the size of a CubeSat.

Currently, various space missions using nanosats and CubeSats have been increasing [3]. As missions using nanosats become a general trend, miniaturization of their components is necessary [4,5]. The orbit of the nanosat can be controlled owing to the miniaturization of propulsion systems, and, thus, a mission that uses the formation flying of nanosats could be conducted [6]. Further, research has been conducted on inter-satellite communication and relative navigation utilizing global positioning system (GPS) signals to use multiple nanosats and CubeSats [7–9]. Most of the multiple nanosat missions using formation flying are technology demonstration missions [10]. For example, CanX-4 and CanX-5 mission, which consists of two 8U nanosats, have performed formation flying to demonstrate control algorithms for autonomous formation maintenance and reconfiguration using an inter-satellite link [11]. The CANYVAL-X mission was to demonstrate an inertial alignment that is a key technology for virtual telescopes [12]. The mission used 1U

\* Corresponding author.

E-mail address: [spark624@yonsei.ac.kr](mailto:spark624@yonsei.ac.kr) (S.-Y. Park).

<https://doi.org/10.1016/j.actaastro.2021.05.013>

Received 15 December 2020; Received in revised form 18 March 2021; Accepted 7 May 2021

Available online 19 May 2021

0094-5765/© 2021 The Authors. Published by Elsevier Ltd on behalf of IAA. This is an open access article under the CC BY-NC-ND license

(<http://creativecommons.org/licenses/by-nc-nd/4.0/>).

Nomenclature			
CanX	Canadian Advanced Nanosatellite eXperiment	$\omega$	argument of perigee
CANYVAL-C	CubeSat Astronomy by NASA and Yonsei using Virtual Telescope Alignment Coronagraph	$\nu$	true anomaly
CANYVAL-X	CubeSat Astronomy by NASA and Yonsei using Virtual Telescope Alignment eXperiment	$M_0$	mean anomaly at epoch
COE	Classical Orbital Element	$n$	mean motion
CPOD	CubeSat Proximity Operations Demonstration	$p$	semi-parameter
EMIC	ElectroMagnetic Ion Cyclotron	$J_2$	gravity coefficient of the J2 perturbation
GMAT	General Mission Analysis Tool	$R_E$	Earth's radius
GomX	GomSpace Express	$\dot{\lambda}$	drift rate
GPS	Global Positioning System	$\lambda$	argument of latitude
GVE	Gauss's variational equation	$\delta\dot{\lambda}_d$	desired change in the drift rate
LEOP	Launch and Early Orbit Phase	$\delta\dot{\lambda}_{imp}$	drift rate changed by the impulse bit
LVLH	Local Vertical and Local Horizontal	$d_{LVLH}$	orbit control direction
MiPS	Micro Propulsion System	$k$	number of remaining commands for station keeping control
MOE	Mean Orbital Element	$T_{ATC}$	along-track correction control time
RAAN	Right Ascension of Ascending Node	$T_{cmd}$	time interval between the control commands
SNIPE	Small-scale magNetosphere and Ionosphere Plasma Experiment	$T_{cont}$	desired orbit control operation time
		$T_{max}$	maximum control operation time
		$t_c$	orbit control epoch
		$t_{min}$	epoch at which the relative distance becomes a minimum
		$t_{OD}$	orbit determination epoch
		$t_{SK1}$	epoch of the initial station keeping control
		$y(t)$	estimated position in the along-track direction
		$Y_{max}$	maximum distance criteria in the along-track direction
		$\dot{y}_{sec}(t)$	secular velocity in the along-track direction
		$\Delta\dot{y}_{burn}$	the effect of the thrust
<b>List of Acronyms</b>			
$a$	semi-major axis		
$e$	eccentricity		
$i$	inclination		
$\Omega$	RAAN		

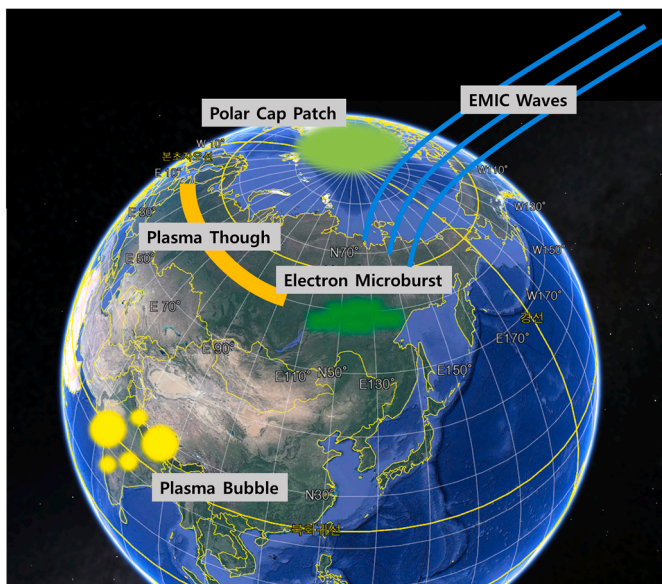


Fig. 1. Observation targets of the SNIPE mission. The targets are located on the equator and latitude of 70° [2].

and 2U nanosats for formation flying. The GomX-4 mission have demonstrated propulsion module, inter-satellite link, chimera board, camera, and star tracker to handle satellite formations using 6U nanosats [13]. The CPOD mission will be launched in 2020 to test rendezvous, proximity operations, and docking with miniaturized components and sensors using 3U nanosats [14]. The CANYVAL-C mission will demonstrate a coronagraph using two CubeSats that perform formation flying using an inter-satellite link [15].

The SNIPE mission utilizes formation flying to observe the temporal and spatial differences in the physical phenomena that exist in the near-

Earth space environment. The mission is not a demonstration mission but an earth science mission using formation flying of four 6U nanosats. It requires four nanosats to observe the same region over time and to observe different regions simultaneously. Kang et al. [2] introduced the candidates for formation flying that fit the SNIPE mission and decided to use along-track and cross-track formations. The formation flying was simulated without constraints and using impulsive burns. Furthermore, they suggested the feasibility of various conceptual formations that satisfy scientific objectives. Otherwise, this study considers nanosat operation and confirms that the proposed formation flying algorithm can effectively control the SNIPE mission orbit. Moreover, specific algorithms for the along- and cross-track formation to be used in actual mission operation were implemented by development and validation. The formation flying scenario presented in Section 2 includes parts that decrease the relative distance between satellites, such as CanX-4 and CanX-5 [16] and GomX-4 missions [17]. The realization of this relative orbit control is necessary for formation flying. Ran et al. [18] studied the relative position coordinated control problem by considering the communication delays between satellites using finite control. Ivanov et al. [19] performed formation flying in the low-Earth orbit using the aerodynamic force. Moreover, the development of a controller that used a nonlinear disturbance observer and asymptotic tracking control for spacecraft-formation flying under unknown external disturbances were reported [20]. In this paper, the formation flying system was designed using the general perturbation theory because the size and shape of formation flying need to be changed over a long time, while considering the delays in communication between the nanosats and the ground station. The proposed design was verified via numerical simulations considering uncertainties.

Unlike these previous missions, the SNIPE mission intends not only to reduce the distance simply by decelerating or accelerating but to gradually approach the minimum distance for a certain duration. Moreover, the SNIPE mission cannot utilize the inter-satellite link that other missions used for the relative navigation to perform autonomous orbit control. Therefore, the orbit control parameters should be derived

based on past orbital information and be applied in the future. The main contribution of this paper is designing the formation flying that satisfies the scientific mission objective, despite the thrust profile being calculated from the ground and transmitted to the nanosat to perform orbit control. In addition, numerical simulations are conducted to verify the formation flying design considering the constraints to implement the intended environment. This study analyzes the constraints and develops orbit control methods. The intended environment should contain the time interval between the orbit determination epoch and the orbit control epoch that arises from ground-based orbit control. In addition, the designed formation flying system should perform the desired orbit control under several constraints. The direction of the orbit control depends on the attitude of the nanosat to ensure that the direction should be fixed during orbit control because attitude control is not possible. Moreover, orbit control should be executed near the equator to secure power stability, and the deployable solar panel should face the Sun during the orbit control. The magnitude of thrust and activating thrust module duration is limited owing to the power consumption. Therefore, we designed and verified a formation flying system that continuously changes shape and size over time to meet the purpose of the scientific mission under several severe constraints.

In this study, we design the shape of the formation, establish the orbit control scenario, analyze the constraints, and validate the system for the SNIPE mission. The remainder of this paper is organized as follows. In section 2, the design of the formation flying system for the SNIPE mission is presented. Two types of formations are devised to collect temporal and spatial data. This section also describes the orbit control scenario to organize the required formation using four nanosats and constraints to reflect the intended environment of the orbit control. Section 3 introduces orbit control methods to overcome the constraints and to operate the required formation flying. Four orbit controls are devised to conduct two types of formations. The nanosats adjust their orbital elements to alter the shape and size of the formations. The attitude of the nanosat at orbit control is discussed in Section 4. Section 5 presents the simulation results to validate the design. It describes from the separation owing to the ejection of four nanosats from the launch vehicle to the end of the mission lifetime. Section 6 contains the conclusions and plans to operate the mission.

## 2. Design formation flying system for the SNIPE mission

### 2.1. Coordinate system

We derived local vertical and local horizontal (LVLH) frames as a relative coordinate system to design the formation flying system as shown in Fig. 2 (a). The origin of the frame is located at the center of mass of the satellite, the fundamental plane is the satellite orbital plane,

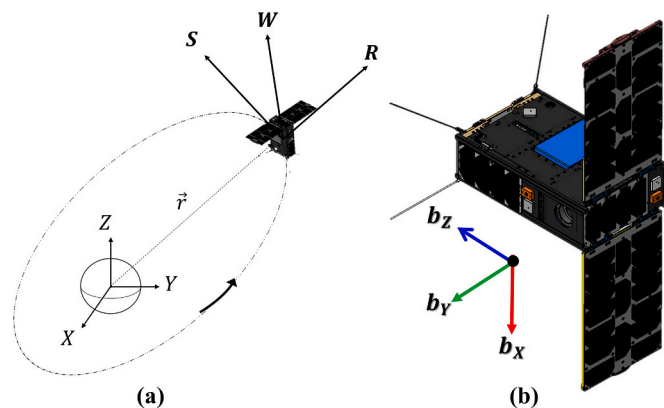


Fig. 2. Definition of local vertical and local horizontal frame, inertial frame (left) and body-fixed frame (right).

and the radial direction (R) is from the Earth to the satellite [21]. The along-track direction (S) is perpendicular to the radial vector and points along the direction of the satellite velocity. The cross-track direction (W) is a direction normal to the orbital plane.

The Earth center inertial coordinate system is expressed as X, Y, Z in Fig. 2 (a) and is used to express an orbit control direction. The origin of the inertial frame is at the center of the Earth, and the fundamental plane is the equatorial plane. X axis points to the vernal equinox, and Y axis is perpendicular with X axis and points to the counter-clockwise direction on the equatorial plane. Z axis points to the North pole [21].

The axes of body-fixed frame of nanosat are  $b_x$ ,  $b_y$ ,  $b_z$  in Fig. 2 (b) and the origin of the frame is the geometric center of nanosat.  $b_z$  axis is the opposite direction of deployable solar panel, and  $b_y$  axis is the opposite direction of thrust module which is the blue box in Fig. 2 (b). The body-fixed frame is used to calculate the attitude of nanosat desired for orbit control.

### 2.2. Top-level requirements of formation flying

There are four major requirements for the formation flying system of the SNIPE mission by allocating the mission requirements. First, four nanosats shall observe the temporal and spatial physical phenomena in space. Second, the system shall gather the four nanosats during the temporal observation phase. Third, the system shall increase the spatial distance between each nanosat during spatial observation. Finally, the system shall generate thrust profile in the ground station. Various sizes and shapes of formations are required to study the mechanism of change on the micro-scale of the Earth's magnetic field. We devised an along-track formation and a cross-track formation to observe temporal and spatial differences, respectively. The along-track formation implies that the nanosats are lined up on the orbital direction of moving of the reference orbit, while the cross-track formation indicates that the nanosats are positioned in the normal direction of the reference orbit. The along- and cross-track directions are defined as the S and W axes in the LVLH frame, respectively, as shown in Fig. 2. When four nanosats are placed on the along-track axis, as shown in Fig. 3 (a), each nanosat passes the same region at different times. Thus, nanosats in this formation can gather the time variation data of the physical phenomena occurring in the same region. The relative distance between nanosats can be modified via orbit controls, thereby facilitating the attainment of different sizes of temporal data. Conversely, when four nanosats are placed on the cross-track axis, as shown in Fig. 3 (b), each nanosat passes a different region on the same latitude simultaneously. Thus, nanosats in the cross-track formation can gather data with regional differences of

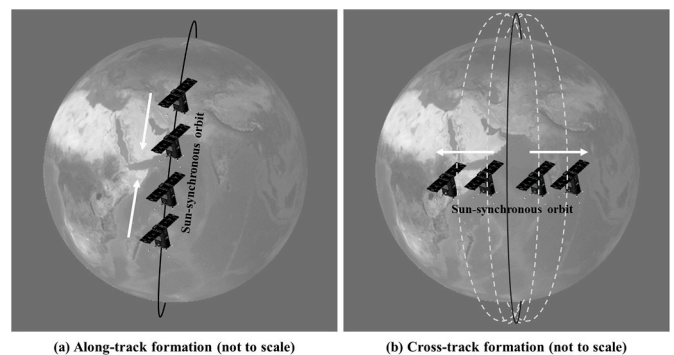


Fig. 3. Concept of the formation flying for SNIPE mission, showing the placement of nanosats in (a) the along-track formation to collect temporal data and (b) in cross-track formation to collect spatial data. The solid line represents the reference orbit, and the dashed lines represent the orbit of nanosats. The orbit of nanosats is similar to the reference orbit in the along-track formation phase. The reference orbit for the cross-track formation represents a propagation of the state vector of reference nanosat at the along-track formation phase.

the same physical phenomena. The formation size can be modified via orbit controls, thereby facilitating the collection of different spatial information. The reference orbit for formation flying corresponds to the Sun synchronous orbit to facilitate the observation of physical phenomena occurring at high latitudes. Since the SNIPE scientific mission does not require a dedicated formation flying, the shapes need not be precisely parallel to the along-track direction or perpendicular to the orbital plane. Even if the shapes are disturbed due to various factors, the purpose of research on the near-Earth space environment can be achieved if the position information of the nanosats that constitute the formation is provided accurately. Thus, the nanosats that make up the formation are located within 40 km in a direction different from that to be aligned with the reference.

2.3. Orbit control scenarios

To alter the sizes and shapes of the formations, nanosats should control their orbit using thrust during the mission lifetime. Fig. 4 describes the changes in the location of the nanosats. Four nanosats separate during the launch and early orbit phase (LEOP), while the nanosats perform nanosat initialization, stabilization, and commissioning the sensors, actuators, and payloads. During the LEOP, the relative distances between nanosats increase by thousands of kilometers. Then, the orbit control scenario for the SNIPE mission consists of four types of orbit control, as shown in Fig. 4. Fig. 4 (a) shows that the relative distances between the nanosats decrease by the maneuvers called drift recovery controls. Four nanosats are brought closer during the along-track formation phase through several finite burns. When the nanosats become close enough to each other, they perform the station keeping controls indicated in Fig. 4 (b) and maintain the relative distance through multiple controls. After finishing the along-track formation phase, the shape of the formation should be switched to enter the cross-track formation phase that collects the spatial information. To transpose the shape, initial configuration controls, corresponding to Fig. 4 (c), are performed. Then, the reconfiguration controls (Fig. 4 (d)) are repeated to increase the size of the cross-track formation at the target regions. The size of the cross-track formation implies the distance between the rightmost and leftmost nanosats along the cross-track direction. Thus, we derived four types of orbit controls, namely, drift recovery, station keeping, initial configuration, and reconfiguration, during the orbit control scenario to operate the two types of formations.

2.3.1. Along-track formation phase

The four nanosats that make up the SNIPE mission will sequentially eject from a single launch vehicle. They move away from each other because of the differences in orbital perturbations for LEOP in which orbit controls are deactivated as described in the flowchart in Fig. 5. For scientific objectives, the relative distance between each nanosat should increase by several thousand kilometers during this phase. Because the direction of ejection could be set from the launch vehicle, the same can be used to increase the size of the along-track formation to several thousand kilometers. According to the concept of operations, the period is expected to be one month. Nanosats move along similar orbital planes and drift apart owing to the differences in orbital drift rate, which is the time variation of the argument of latitude. The distance between nanosats could be thousands of kilometers. After orbit control becomes available, the along-track formation begins by performing drift recovery control that reduces the relative distance between the nanosats. The control could be performed several times because of thrust limitations and control errors. During the data collection phase of temporal differences, the relative distance between each nanosat is reduced from thousands of kilometers to less than tens of kilometers. Thus, these nanosats can be made to come closer steadily for 3 months during the along-track formation phase. Several temporal data can be obtained owing to this change in the relative distance. The formation flying system shall maintain the relative distance to prevent the nanosats from

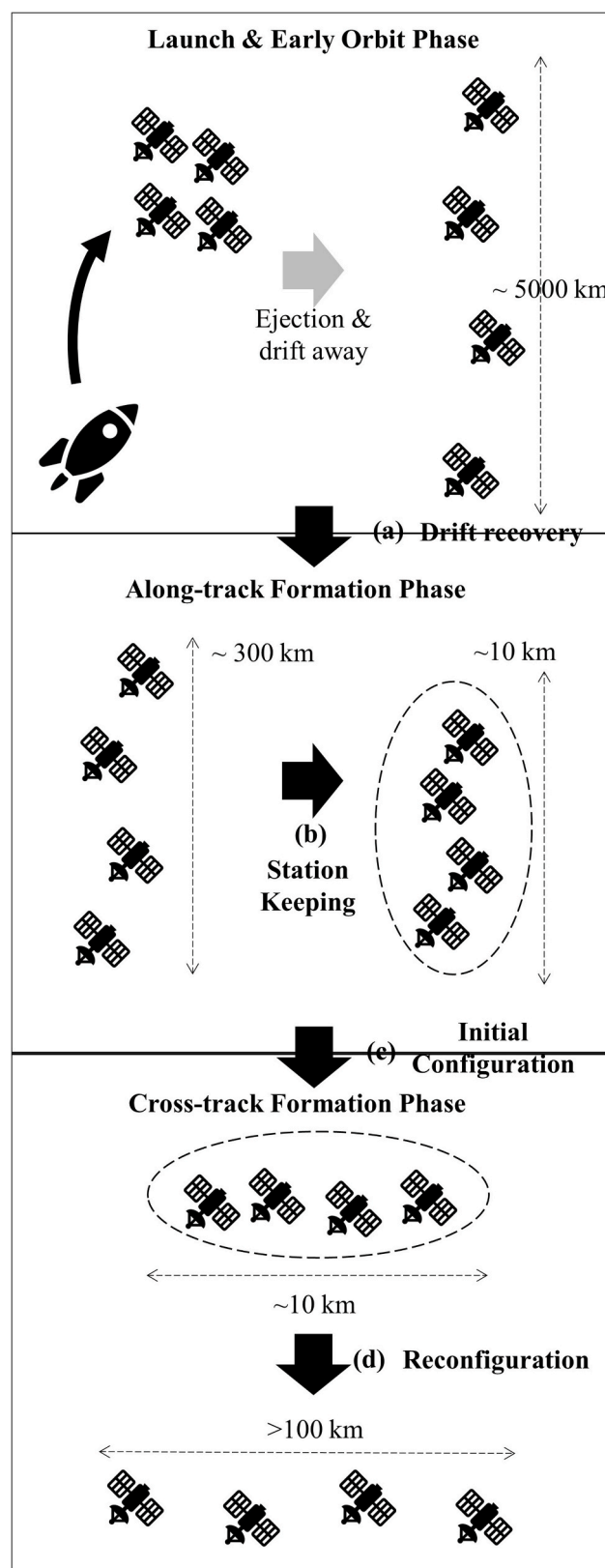


Fig. 4. Change in the shape and size of the formation conducted by the four nanosats. Nanosats initially form the along-track formation and transpose to the cross-track formation. The relative distances between nanosats can be decreased and increased during along-track and cross-track formations, respectively, via orbit controls in the desired duration.

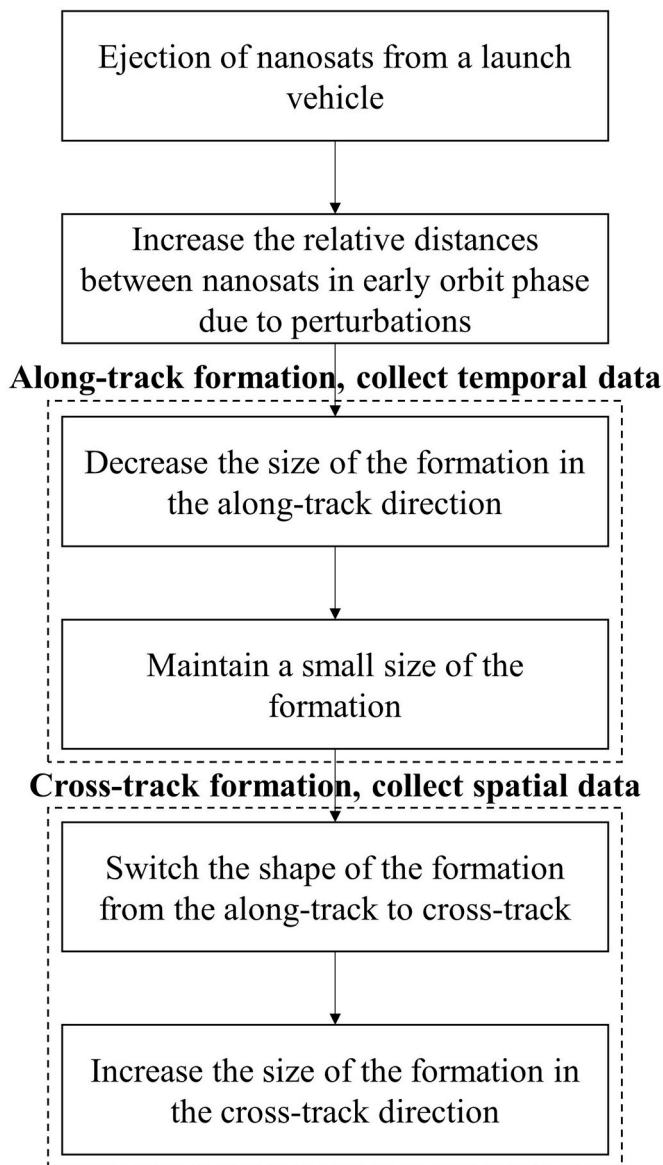


Fig. 5. Sequence of changes in formation shape and size. Orbit controls decrease and increase the along-track and cross-track formation sizes to collect temporal and spatial data, respectively.

passing through each other. The station keeping control is started considering the relative speed and distance. The control is conducted to regulate the drift rate to maintain small relative distances between the nanosats. The control also adjusts the relative velocity through multiple attempts to reduce the change in relative distance owing to control errors. The along-track formation phase lasts 3 months to observe the temporal data of physical phenomena as shown in Fig. 5, and the relative distance decreases to tens of kilometers at the end of this phase.

### 2.3.2. Cross-track formation phase

After the four nanosats finish the station keeping controls, the shape of the formation is transposed to observe the spatial differences in the cross-track formation using the initial configuration controls. Two nanosats change their inclinations to obtain the relative distance at high latitudes, and others change their right ascension of ascending nodes (RAANs) to obtain the size of the formation at the equator. Since a single finite burn cannot change the shape of the formation due to the limitation in time to generate enough thrust, the alternation of the formation is completed through repeated initial configuration controls for several

days. After switching the shape of formation, four nanosats control their orbit to extend the size of the cross-track formation. The cross-track formation shall progressively expand by over 100 km at the equator and cover a latitude of  $70^\circ$  over 3 months. The size of the cross-track formation expands by moving the relative distances away in the cross-track direction through repeated inclination changes using the reconfiguration controls. The reconfiguration control increases the formation size by rearranging the nanosat positions. The size gradually increases to more than 100 km at the equator and a latitude of  $70^\circ$  in three months. During this cross-track formation, the SNIPE mission collects spatial data of the targeted physical phenomena as shown in Fig. 5.

### 2.4. Constraints on formation flying

There are several constraints on orbit controls, such as the time interval between orbital knowledge data and orbit control commands, limitation in attitude control, power safety of nanosat, and errors caused by the specifications of the thrust module. Therefore, the constraints and devised control methods that allow for the desired orbit controls even with these constraints should be analyzed. In addition, simulations for the orbit controls should consider these constraints, which implement the intended environment of the orbit control, to validate the formation flying system design. The intended environment corresponds to the actual nanosat operating conditions.

#### 2.4.1. Time difference between orbit determination data and orbit control epoch

The communication between the user and each nanosat is performed once per day owing to the limitation of the ground station. The SNIPE team could only construct a single ground station at a latitude of  $37^\circ$  in South Korea; therefore, the communication duration is expected to be less than 15 min per contact. The orbit control parameters must be derived in the ground station based on the orbital information received from the nanosats because the nanosats cannot use the inter-satellite link. Fig. 6 illustrates the time interval between the orbital information and the orbit control command. In the first communication, the operation team receives telemetry with GPS data of the nanosat and performs precise orbit determination to check the results of previous orbit control. In the second communication, the team calculates the orbit control parameters based on precise orbit determination results that are derived based on the GPS data from this communication. Since the nanosat has already passed over the coverage of the ground station during the calculation and examination stages, the team should transmit the orbit control command on the third communication. Consequently, the orbit control parameters that are executed in the future should be calculated based on past orbital information. The time interval between orbit control commands is more than three days.

#### 2.4.2. Limitation in the thrust direction for orbit controls

The orbit control direction depends on the attitude of the nanosat. All four nozzles in the thrust module are in the same direction ( $-b_y$ ) as described in Fig. 7; hence, the thrust module can only generate control acceleration in one direction. However, the attitude cannot be changed during orbit control because the torque generated by the misalignment in the thrust module and the torque from the reaction wheel are coupled. To facilitate attitude changes, the reaction wheel must generate the desired torque; however, it is impossible to change the attitude in a desired direction due to the disturbance torque generated by the thrust misalignment, which exceeds the capacity of the reaction wheel. Because the orbit-control direction depends on the nanosat attitude and the attitude cannot be changed during thruster firing, the thrust direction for orbit control remains fixed in the inertial frame as described in Fig. 8. The pointing accuracy affects the direction error of  $\Delta V$ , which is predicted to be  $10^\circ$  ( $3\sigma$ ) in the simulations. In addition, the imbalance between the magnitude of thrust, which is generated from each nozzle, causes torque, and varies in the attitude of the nanosat. Therefore, the

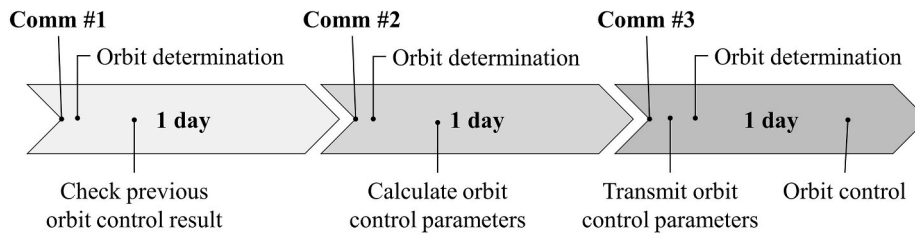


Fig. 6. Timeline in orbit control command. A single orbit control command requires at least three communications (i.e., 3 days) between the user and each nanosat.

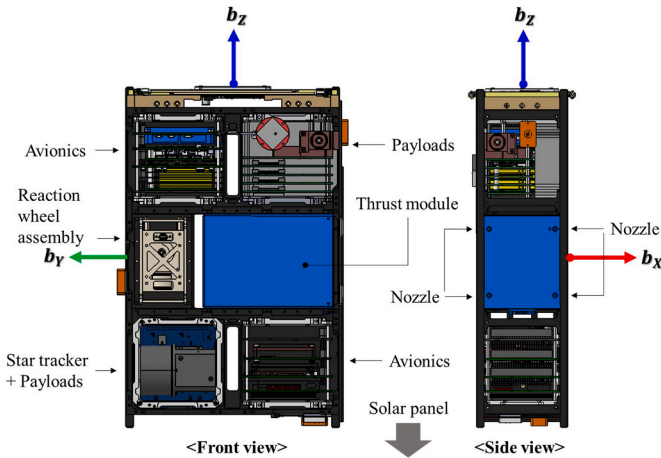


Fig. 7. Location and shape of the thrust module. The blue box in the middle of nanosat is the thrust module. The module is mounted in the middle of nanosat and the thrust direction is in  $-b_y$  axis of body frame. The four black dots in the middle of the thrust module on the side view image are thrust nozzles. The deployable solar panel faces in the  $-b_z$  direction. (For interpretation of the references to colour in this figure legend, the reader is referred to the Web version of this article.)

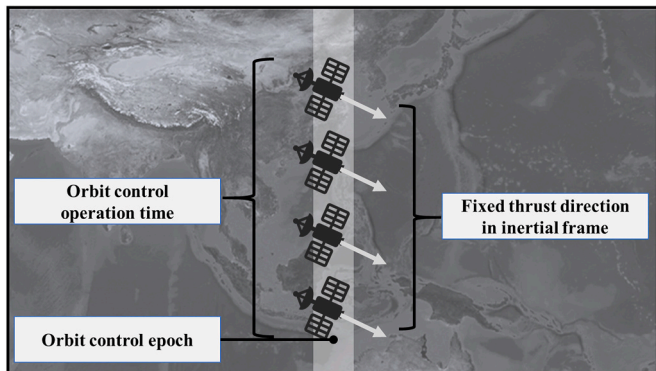


Fig. 8. Conceptual image illustrating thrust generation along a fixed direction in the inertial frame during orbit control operation time.

thrust modulation algorithm, which turn each nozzle on and off based on the direction error, is required to reduce the direction error while activating the thruster module.

2.4.3. Power safety of the nanosat for orbit controls

Three constraints are considered to secure the power stability of a nanosat because the heater which is mounted on the thrust module to vaporize fuel consumes a significant amount of power in a short time. First, there is a limitation in the time required to activate the thrust module. Therefore, orbit control should be performed for a certain duration and several times for each type of orbit control. Second, the

orbit controls should be preferred to be executed on the equator on the dayside. The deployable solar panel is attached on the top of the nanosat on the  $-b_z$  axis, and the nanosat is pointing to the Sun to charge the battery before the orbit controls. Nanosat should control its attitude to generate acceleration in the desired direction before activating the thrust module. Therefore, maneuvers shall be performed near the equator to minimize the change in attitude for the orbit control when the fuel consumption does not increase significantly. Third, the deployable solar panel should face the Sun to the extent possible during orbit controls.

2.4.4. Specification of the thrust module

Nanosats mount a customized micro propulsion system (MiPS) produced by VACCO Industries, USA. The specifications of the thrust module are listed in Table 1. The SNIPE team expanded the propellant tank to get more total  $\Delta V$ ; thus, the total size of the thrust module for the SNIPE mission became 1.5U as shown in Fig. 7. Because of the specification of the thrust module, the magnitude of the impulse bit is fixed at 25 mNs per thrust nozzle. The thrust magnitude error could be 20% (Table 1); hence, it causes an error in the orbit controls. The magnitude of  $\Delta V$  per second generated from the thrust module is constant at 0.01 m/s when the mass of the nanosat is 10 kg. The  $\Delta V$  budget of each nanosat is shown in Table 2, and the total  $\Delta V$  of the thrust module is 50 m/s with a margin of 20%. Since the drift recovery and the station keeping are the controls on the orbital plane, the  $\Delta V$  consumption is small. Otherwise, the initial configuration and reconfiguration change the orbital plane, so they require more  $\Delta V$  than the controls on the orbital plane.

3. Orbit control methods for formation flying

In this paper, analytical control methods using general perturbation theory were presented. The perturbations considered during simulations performed in this study were not considered at the design stage because their effect was insignificant compared to the J2 perturbations considered during design. Moreover, the integrated effect of the air drag was found to be similar because nanosats of the same shape move in nearly similar orbits. So, the orbit control methods only consider J2 perturbation in the design stage. Fig. 9 depicts a comprehensive flowchart of the orbit control methods. The nanosats modulate the drift rate during the along-track formation to decrease and maintain their relative distance. They change their inclination or RAAN for increasing the size of the cross-track formation while maintaining the along-track size via the

Table 1 Specification of MiPS thrust module.

Contents	Specification
Propellant (cold gas)	R-236fa
Thruster	4 RCS
Nozzle alignment	$\leq \pm 1$ degree
Thrust	25 mN $\pm$ 5 mN
Total impulse	503 Ns
Dry mass	963 g
Propellant mass	1314 g

**Table 2**  
 $\Delta V$  budget of each nanosat in the SNIPE mission.

Formation type	Control type	$\Delta V$ budget (m/s)
Along-track formation	Drift recovery	3
	Station keeping	2
Cross-track formation	Initial configuration	12
	Reconfiguration	23
Margin		10
Total		50

along-track correction control. The general perturbation theory was used to derive the orbit control algorithms for the formations. The along-track formation was operated based on the drift rate equation, and the secular change in the argument of latitude occurred due to the  $J_2$  perturbation. The cross-track formation was operated based on the secular change of RAAN by  $J_2$  perturbation. Since the effect of the  $J_2$  perturbation varies according to the orbital elements, Gauss's variational equations (GVEs) were introduced to control the orbital elements. Nanosats cannot use inter-satellite communication, so the orbit control parameters must be calculated from the ground. Because the attitude cannot be changed while performing orbit control, the thrust must be generated in a fixed direction. In addition, the magnitude of the thrust that the thrust module can generate is fixed; in other words,  $\Delta V$  that can be generated in 1 s is fixed. Therefore, the magnitude of the control is expressed in time. Orbit control parameters to be calculated from the ground and transmitted to the nanosats are the orbit control direction, orbit control operation time, and orbit control epoch. The direction is determined as the most efficient direction, and the time is determined in consideration of the thrust operation period according to the power. The epoch is determined to ensure that the nanosat is located at the reference latitude in the middle of the orbit control operation time. This allows the nanosats to generate a fixed thrust along the determined orbit control

direction during the derived orbit control operation time from the calculated orbit control epoch.

**3.1. Drift recovery control for the along-track formation**

The drift recovery control is used to decrease the size of the formation to observe different scales of temporal data during the along-track formation phase. The maneuvers change the orbital drift rate to adjust the relative velocity, which decreases the relative distance between the nanosats. The drift rate ( $\dot{\lambda}$ ) donates the change in the argument of latitude. It is the sum of the mean motion ( $n$ ), the change in argument of perigee ( $\dot{\omega}$ ), and mean anomaly at epoch ( $M_0$ ) caused by the  $J_2$  orbital perturbation. This implies that, at an orbital angular rate, the satellite moves on the orbital plane. It is a function of the semi-major axis ( $a$ ), eccentricity ( $e$ ), and inclination ( $i$ ), as expressed in Eq. (1) [22]. The equation for the drift rate is expressed as follows:

$$\dot{\lambda}(a, e, i) = \dot{\omega} + \dot{M}_0 + n = \frac{3n J_2 R_E^2}{4p^2} (4 - 5\sin^2 i) + \frac{3n J_2 R_E^2 \sqrt{1 - e^2}}{4p^2} (2 - 3\sin^2 i) + \sqrt{\frac{\mu}{a^3}} \tag{1}$$

where  $\lambda$  is the argument of latitude,  $J_2$  is the gravity coefficient of the  $J_2$  perturbation,  $R_E$  is the Earth's radius,  $\mu$  is the gravitational parameter for Earth, and  $p = a(1 - e^2)$  is a semi-parameter. The drift rate was calculated based on the Brouwer long mean orbital elements (MOEs) to reduce the standard deviation of the drift rate caused by the orbital motion. The standard deviation was larger than the desired change in the drift rate when the drift rate of the nanosat was derived based on the classical orbital elements (COEs). The use of MOEs can ignore periodic oscillations that do not affect the mission [23]. The desired change in the drift rate ( $\delta\dot{\lambda}_d$ ) of the deputy nanosat was

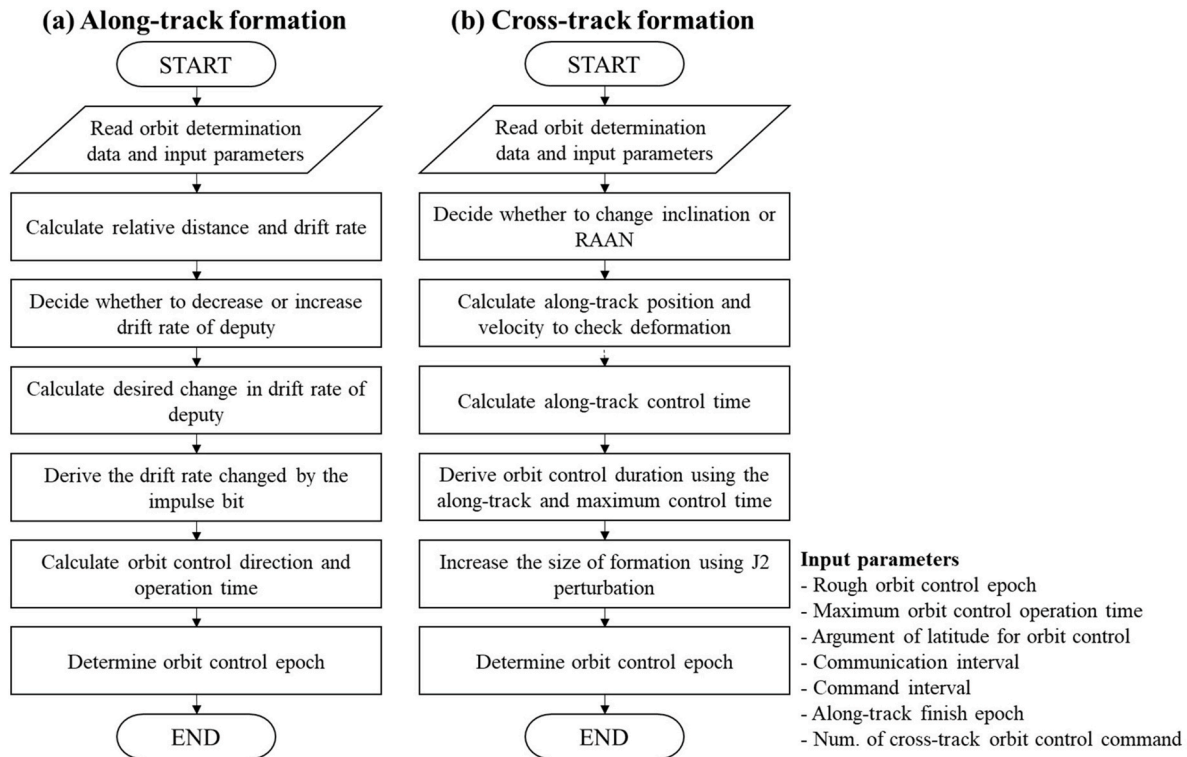


**Fig. 9.** Comprehensive flow-chart of the orbit control strategy. (a) Is for the along-track formation that changes the drift rate, and (b) is for the cross-track formation that changes inclination or RAAN.

$$\delta\dot{\lambda}_d = \begin{cases} -\frac{2\pi + \Delta\lambda}{T_{DR}} & , -2\pi \leq \Delta\lambda < -\pi \\ -\frac{\Delta\lambda}{T_{DR}} & , -\pi \leq \Delta\lambda \leq \pi \\ \frac{2\pi + \Delta\lambda}{T_{DR}} & , \pi < \Delta\lambda < 2\pi \end{cases} \quad (2)$$

where  $\Delta\lambda = \lambda_{dep} - \lambda_{ref}$  is the difference in the argument of latitude between the reference nanosat ( $0 \leq \lambda_{ref} < 2\pi$ ) and deputy nanosat ( $0 \leq \lambda_{dep} < 2\pi$ ) and  $T_{DR}$  is the remaining time of the along-track formation phase. To minimize the change in the drift rate, it was calculated by dividing the range, as in Eq. (2). Based on the difference in the argument of latitude between the two nanosats, the increase or decrease in the drift rate of the deputy nanosat can be determined to minimize the desired change in drift rate. The desired change in the drift rate was calculated to reduce the relative distance in the desired duration for the temporal observations. This duration corresponds to two to three

$$\begin{aligned} \delta\Omega &= \frac{\sqrt{1-e^2}\sin\lambda}{na(1+e\cos\nu)\sin i}\Delta V_W, \\ \delta\omega &= \frac{\sqrt{1-e^2}}{nae} \left\{ -\cos\nu\Delta V_R + \frac{\sin\nu(2+e\cos\nu)}{1+e\cos\nu}\Delta V_S \right\} \\ &\quad + \frac{\sqrt{1-e^2}}{na(1+e\cos\nu)}\cot i\sin\lambda\Delta V_W, \\ \delta M_0 &= \frac{1-e^2}{nae} \left\{ \left( \cos\nu - \frac{2e}{1+e\cos\nu} \right)\Delta V_R + \frac{2+e\cos\nu}{1+e\cos\nu}\sin\nu\Delta V_S \right\}, \end{aligned}$$

where  $\nu$  is the true anomaly;  $\Delta V_R$ ,  $\Delta V_S$ , and  $\Delta V_W$  are components of  $\Delta V$  in the radial, along-, and cross-track directions, respectively; and  $\Omega$  is the RAAN. Therefore, the drift rate changed by the impulse bit ( $\delta\dot{\lambda}_{imp}$ ) was derived by combining Eqs. (3) and (4).

$$\delta\dot{\lambda}_{imp} = \begin{bmatrix} \frac{\partial\dot{\lambda}}{\partial a} & \frac{\partial\dot{\lambda}}{\partial e} & \frac{\partial\dot{\lambda}}{\partial i} \end{bmatrix} \begin{bmatrix} \frac{2e\sin\nu}{n\sqrt{1-e^2}} & \frac{2(1+e\cos\nu)}{n\sqrt{1-e^2}} & 0 \\ \frac{\sqrt{1-e^2}\sin\nu}{na} & \frac{\sqrt{1-e^2}}{na} \left( \cos\nu + \frac{e+\cos\nu}{1+e\cos\nu} \right) & 0 \\ 0 & 0 & \frac{\sqrt{1-e^2}\cos\lambda}{na(1+e\cos\nu)} \end{bmatrix} \begin{bmatrix} \Delta V_R \\ \Delta V_S \\ \Delta V_W \end{bmatrix} \quad (5)$$

months in accordance with the concept of operations.

The orbit control operation time was calculated by estimating the drift rate that is changed by  $\Delta V$ . When the drift rate equation is linearized by the semi-major axis, eccentricity, and inclination, it is shown in Eq. (1) that the change in the drift rate described in Eq. (3) depends on the change in the orbital elements.

$$\delta\dot{\lambda} = \frac{\partial\dot{\lambda}}{\partial a}\delta a + \frac{\partial\dot{\lambda}}{\partial e}\delta e + \frac{\partial\dot{\lambda}}{\partial i}\delta i.$$

with

$$\frac{\partial\dot{\lambda}}{\partial a} = \frac{21J_2R_E^2\sqrt{\mu}}{8(1-e^2)^2a^{9/2}}(4-5\sin^2i) + \frac{21J_2R_E^2\sqrt{\mu}}{8(1-e^2)^{3/2}a^{9/2}}(2-3\sin^2i) + \frac{3\sqrt{\mu}}{2a^{5/2}}, \quad (3)$$

$$\frac{\partial\dot{\lambda}}{\partial e} = \frac{3J_2R_E^2e\sqrt{\mu}}{a^{7/2}(1-e^2)^3}(4-5\sin^2i) + \frac{9J_2R_E^2e\sqrt{\mu}}{4a^{7/2}(1-e^2)^{5/2}}(2-3\sin^2i),$$

$$\frac{\partial\dot{\lambda}}{\partial i} = \frac{3J_2R_E^2\sqrt{\mu}}{4a^{7/2}(1-e^2)^2}(-5-3\sqrt{1-e^2})\sin 2i.$$

In this study, we used Gauss's variational equations (GVEs) to represent the variation in orbital elements due to an external force to confirm the change in the orbital element due to the fixed thrust. The change in drift rate due to  $\Delta V$  can be calculated using the time discretized GVEs and Eq. (3). The discretized GVEs can be expressed as [24]:

$$\delta a = \frac{2}{n\sqrt{1-e^2}} \{ e \sin\nu\Delta V_R + (1+e\cos\nu)\Delta V_S \},$$

$$\delta e = \frac{\sqrt{1-e^2}}{na} \left\{ \sin\nu\Delta V_R + \left( \cos\nu + \frac{e+\cos\nu}{1+e\cos\nu} \right)\Delta V_S \right\},$$

$$\delta i = \frac{\sqrt{1-e^2}\cos\lambda}{na(1+e\cos\nu)}\Delta V_W, \quad (4)$$

As discussed in the previous section, the orbit controls shall be executed near the equator to minimize the alteration in attitude. Therefore, the orbit control direction was determined to be the direction that has the maximum effect on the drift rate among the three axes of the LVLH frame. In addition, the direction must be fixed on the inertial frame because the direction depends on the attitude of the nanosat and the attitude cannot be controlled during thrust generation. Therefore, the orbit control direction calculated from the LVLH frame based on the equator was converted into an inertial frame. The direction expressed in the inertial frame is used to calculate the desired attitude of the nanosat for orbit control. Because  $\Delta V$  was fixed by the specification of thrust module, a drift rate that was changed by the thrust generated for a second ( $\delta\dot{\lambda}_{imp}$ ) can be calculated when thrust was generated in the most efficient direction. Further, the desired orbit control operation time ( $T_{cont.DR}$ ) was calculated by dividing the desired change in drift rate ( $\delta\dot{\lambda}_d$ ) by the change in the drift rate by the impulse bit ( $\delta\dot{\lambda}_{imp}$ ).

$$T_{cont.DR} = \frac{\delta\dot{\lambda}_d}{\delta\dot{\lambda}_{imp}} \quad (6)$$

If the calculated orbit control operation time exceeds the maximum orbit control operation time, which was set to 30 s in the simulation, the orbit control was performed only for the maximum time, and then the same type of orbit control was executed in the next chance.

### 3.2. Station keeping control for the along-track formation

Station keeping control aims to maintain the relative distance between nanosats to prevent the nanosats from passing through each other at the final stage of the along-track formation. It also aims to make render the drift rates of both nanosats equal. The maneuvers make the drift rate of the deputy equal to the drift rate of the reference. Therefore, the desired change in the drift rate of the deputy nanosat was

$$\delta\dot{\lambda}_d = \dot{\lambda}_{ref} - \dot{\lambda}_{dep}, \quad (7)$$

where  $\dot{\lambda}_{dep}$  is the drift rate of the deputy nanosat and  $\dot{\lambda}_{ref}$  is the drift rate of the reference nanosat calculated based on MOEs. The control should be performed by splitting it several times to reduce the change in relative distance after finishing the along-track formation phase caused by the magnitude error and direction error of the thrust. The epoch of the initial station keeping control ( $t_{SK1}$ ) was determined based on the remaining duration for the along-track formation phase and expected command times for the station keeping control. The epoch is

$$t_{SK1} = t_{min} - \frac{k-1}{2} T_{cmd}, \quad (8)$$

where  $t_{min}$  is the epoch at which the relative distance becomes a minimum if orbit control is not performed,  $k$  is the number of remaining commands for station keeping control that are determined by the concept of operations, and  $T_{cmd}$  is the time interval between the control commands that was set to 5 days in the simulation. The orbit control direction was considered the most efficient axis in the LVLH frame, similar to the drift recovery control. The orbit control operation time ( $T_{cont,SK}$ ) was calculated in the same manner as the drift recovery controls. However, it was divided more by the number of remaining commands for the station keeping control, as expressed in Eq. (9).

$$T_{cont,SK} = \frac{\delta \dot{\lambda}_d}{k \delta \dot{\lambda}_{imp}} \quad (9)$$

After the final station maintains control, the distance between nanosats could be less than 10 km, and the corresponding relative speed will be less than 10 km/day.

### 3.3. Initial configuration control for the cross-track formation

The initial configuration controls switch the shape of the formation flying from the along-track formation to the cross-track formation to observe the spatial differences of the physical phenomena in the geomagnetic field. To switch from the along-track formation to the cross-track formation, two nanosats changed their inclinations and the other two changed their RAAN. The change in inclination and RAAN by  $\Delta V$  is shown in GVEs, Eq. (4). Spatial difference data at latitude of  $70^\circ$  can be collected by two nanosats with different inclinations. As the difference in inclinations of two nanosats increases, the relative distance increases geometrically at the high latitudes as described in Fig. 10 (a). Otherwise, the data at the equator can be collected by the other two nanosats which have different RAANs. As the difference in RAANs of two nanosats increases, the relative distance increases geometrically at the

equator as described in Fig. 10 (b). One nanosat increased its inclination, and the other nanosat decreased its inclination. Similarly, the other two nanosats changed the RAAN to switch the shape of the formation. After the initial configuration controls, four nanosats can be aligned in the normal direction of the orbital plane, as described in Fig. 10 (c), at a latitude of  $70^\circ$ . This shape of formation, cross-track formation, can gather the science data in spatial differences around the latitude of  $70^\circ$ .

To minimize  $\Delta V$  consumption, controls to change the inclination and RAAN should be conducted at the equator and poles, respectively. As expressed in Eq. (4), the change in inclination by  $\Delta V$  is a function of  $\cos \lambda$  such that the controls should be performed at the points where the argument of latitude is  $0^\circ$  or  $180^\circ$  to minimize  $\Delta V$  consumption and maximize change in inclination. Similarly, the change in RAAN by  $\Delta V$  is a function of  $\sin \lambda$  such that the controls should be performed at the points where the argument of latitude is  $90^\circ$  or  $270^\circ$ . Therefore, orbit controls to change the RAAN are performed near the pole to reduce fuel consumption. It was preferred to perform orbit control near the equator to minimize the variation in attitude for orbit control, but the control to change RAAN was performed at the pole to minimize  $\Delta V$  consumption. In addition, the thrust should act in the cross-track direction to change the inclinations and RAANs. Changing orbital plane consumes a significant amount of fuel. This indicates that switching the shape of formation requires a long orbit control operation time. Therefore, the initial configuration controls were performed repeatedly several times until the size of the cross-track formation became more than 10 km and were executed for the maximum control operation time, which was set to 100 s in the simulation at each command.

According to the drift rate equation, Eq. (1), the difference in inclinations resulted in differences in the drift rate, which changes the relative distance in the along-track direction. In addition, the thrust should be activated in the cross-track direction, but the direction error of the thrust causes  $\Delta V$  to act in an unintended direction. Therefore, the distance in the along-track direction was not maintained and should be corrected to maintain the cross-track formation. Therefore, the along-track correction control was needed to reduce the deformation of the cross-track formation in the along-track direction. The amount of control for the along-track correction control was expressed in time. The along-track correction control time ( $T_{ATC}$ ) was obtained based on the estimated position in the along-track direction at the control epoch ( $y(t_c)$ ) and the effect of the thrust ( $\Delta y_{burn}$ ) derived from the controls in the along-track formation phase. The along-track correction control time ( $T_{ATC}$ ) was

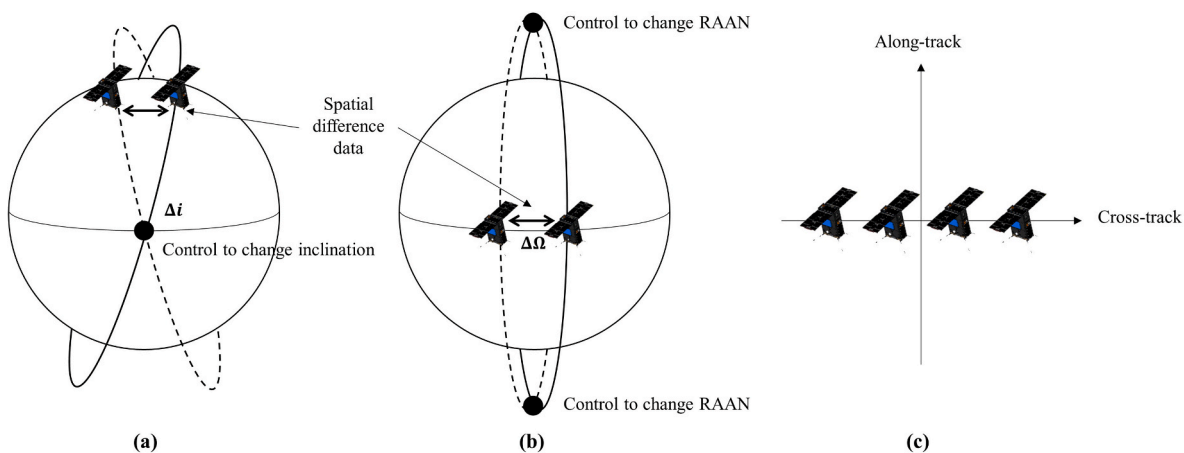


Fig. 10. Conceptual image illustrating how difference between inclination and RAAN ensures relative distance along spatial direction: Inclination change reserves the spatial distance at  $70^\circ$  latitude, whereas RAAN change reserves spatial distance at equator.

$$T_{ATC} = \begin{cases} \frac{\dot{y}_{sec}(t_{OD})}{\Delta\dot{y}_{burn}}, & y(t_c) < y_{max} \\ \frac{\dot{y}_{sec}(t_{OD}) + \frac{y(t_c)}{T_{cmd}}}{\Delta\dot{y}_{burn}}, & y(t_c) \geq y_{max} \end{cases}, \quad (10)$$

where  $t_c$  is the orbit control epoch,  $t_{OD}$  is the orbit determination epoch, and  $y_{max}$  is the maximum distance criteria in the along-track direction, which is set to 10 km. When the estimated position at the control epoch ( $y(t_c)$ ) was less than  $y_{max}$ , the control succeeded to reduce the relative velocity in the along-track direction. However, if the position exceeded the maximum distance, the control operated to make the distance in the along-track direction zero at the next control epoch, as expressed in Eq. (10). Here,  $\dot{y}_{sec}(t)$  is the secular velocity in the along-track direction at the epoch.  $\dot{y}_{sec}(t)$  was derived at the orbit determination epoch based on the precise orbit determination data because the orbit control parameters shall be calculated on the ground station based on the received data from the nanosats. When the relative coordinate system was constructed using orbit prediction data after a day or more, the errors in position and velocity were too large to correct the deformation in the along-track direction owing to orbit propagation errors. Therefore, the deformation at the orbit control epoch was predicted using a state vector on the relative coordinate system constructed using precise orbit determination data. If  $T_{ATC}$  is more than 10 s, it is judged that the relative speed is not sufficiently small; thus, the station keeping control should be conducted.

The orbit control direction of the initial configuration control was determined by the combination of the inclination or RAAN change control and the along-track correction control. The direction should be fixed during the orbit control; thus, it was calculated at the equator when changing the inclination and at the pole when changing the RAAN. The along-track correction control should act in the along-track direction, and orbital elements change control should act in the cross-track direction. Because the required magnitude of control is expressed in time, the orbit control direction is calculated with the combination of along-track correction control time and orbital plane change control time. As thrust is generated during the maximum orbit control time, the direction is determined to ensure that the thrust acts in the along-track direction for along-track correction control. Therefore, the orbit control direction ( $d_{LVLH}$ ) was directly obtained from the along-track control time and maximum control operation time ( $T_{max}$ ) as

$$d_{LVLH} = \begin{bmatrix} 0 & \frac{T_{ATC}}{T_{max}} & \frac{\sqrt{T_{max}^2 - T_{ATC}^2}}{T_{max}} \end{bmatrix}. \quad (11)$$

The maximum control operation time was set to 100 s according to the power stability. The direction implies that the amount of control required for the along-track correction acts in the along-track direction, and the remaining amount of control is used to change the inclination or RAAN. The direction should be fixed during the thrust firing; subsequently, the direction calculated from the LVLH frame based on the equator or poles was converted into an inertial frame. The input maximum control operation time was used as the orbit control operation time. Orbit control started to pass through a node or pole in the middle of the orbit control operation time on the dayside. Therefore, the direction was derived on the inertial frame, the control operation time was the maximum control operation time, and the epoch was before the nanosat passed the node or pole.

### 3.4. Reconfiguration control for cross-track formation

The reconfiguration control consistently extends the size of the cross-track formation to satisfy the scientific objective. In the cross-track formation phase, the nanosats slightly changed the orbital plane to increase the observation interval of the spatial data. After the initial

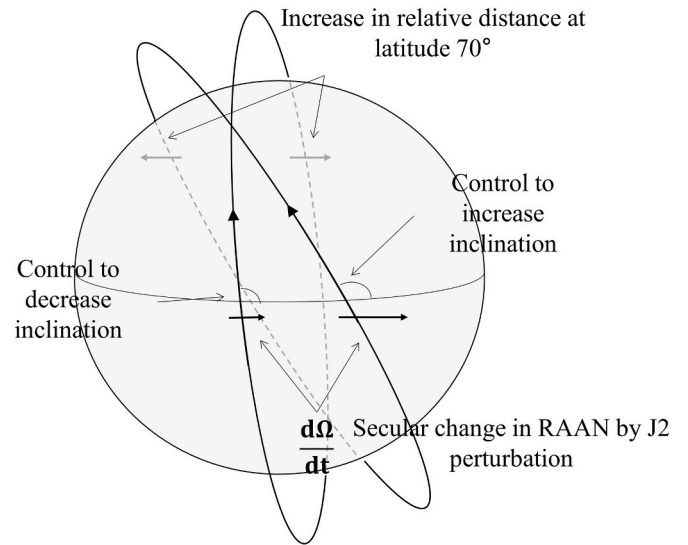


Fig. 11. Concept of the reconfiguration control. Inclination is changed by the orbit control and RAAN is naturally changed by the J2 orbital perturbation.

configuration control that changed from the along-track formation to the cross-track formation, all nanosats changed their inclinations to increase the size of the formation. The two nanosats with a small RAAN decreased their inclinations, while the other two with a large RAAN increased their inclinations. The controls were executed near the equator. In addition, increasing the size utilized the secular change in RAAN owing to the J2 perturbation. The secular rate in RAAN by J2 perturbation can be found in Ref. [21].

$$\frac{d\Omega}{dt} = \frac{3J_2 R_E^2 n \cos i}{2a^2(1-e^2)} \quad (12)$$

Fig. 11 describes how to increase the size of the cross-track formation through reconfiguration control. When the inclination was more than 90°, increasing the inclination increased the magnitude of the secular rate of RAAN, and decreasing the inclination decreased it. This increased the relative distance on the equator, as shown in Fig. 11. The difference in RAAN naturally increased over time because of the secular variation of RAAN, which is caused by the J2 orbital perturbation. Therefore, at the equator, the size of the cross-track formation consistently expanded owing to the secular variation of RAAN with changing inclination. In addition, the size of the formation expanded as the difference in inclination and RAAN increased at the latitude of 70°, as shown in Fig. 11. The difference between inclinations also caused deformation in the along-track direction because of the difference in drift rates between nanosats. Therefore, the along-track correction control was also needed during the cross-track formation phase, similar to the initial configuration controls.

To perform ground-based orbit control, we must calculate when, in which direction, and how long the thrust to be activated. The control epoch was determined before the nanosat passed the ascending or descending node on the dayside. The control was initiated to ensure that the node came in the middle of the control operation time. The reconfiguration control included cross-track direction control to increase the size of the cross-track formation and along-track correction control to maintain the shape of the formation. Therefore, the orbit control direction for the reconfiguration control was determined with the combination of the orbital element change control and the along-track correction control, which was similar to the initial configuration controls. The control operation time was also set with the input maximum control operation time.

### 4. Attitude of the nanosat for orbit controls

#### 4.1. Attitude calculation of the nanosat for orbit controls

In this study, the TRIAD method is used to calculate the desired nanosat attitude on the ground for the solar panel to face the Sun to the extent possible to ensure power stability during the orbit controls. As the solar panel must face the Sun to the extent possible while the thrust direction of the nanosat is in the direction of orbit control, the attitude of the nanosats during orbit control is calculated using the TRIAD method. The TRIAD method is one of the simplest static attitude determination methods, requiring only two vector measurements [25]. The TRIAD method was used to generate the desired attitude that the nanosat should achieve during thrust generation. The attitude requirement for this situation was that the thrust direction was aligned exactly with the desired orbit control direction, while the angle between the Sun and solar panels was minimized to the extent possible for power generation. Owing to the aforementioned features of the TRIAD method, it can be used to calculate the attitude satisfying the requirement by aligning the desired thrust vector in the inertial frame with the thrust direction in the body-fixed frame and mapping the Sun vector in the inertial frame to the solar panel direction in the body-fixed frame.

To inspect the adequacy of the TRIAD method for this situation, sets of sun vectors and desired thrust vectors in the inertial frame were generated, and the rotation matrix was calculated via the TRIAD method for each set of data. The thrust direction vector was  $[0 -1 0]$ , and the solar panel direction vector was  $[0 0 -1]$  on the body-fixed frame, as shown in Fig. 7. We converted the two vectors on the body-fixed frame to the inertial frame using the rotation matrix calculated from the TRIAD method and compared them with the Sun vector and orbit control vector on the inertial frame. As shown in Fig. 12, the angles between the thrust direction vector and the desired orbit control vector were zero. However, the angles between the solar panel direction vector and the Sun vector were not zero for all datasets. The reason for these differences is the mutual perpendicularity of the thrust and solar panel direction vector frames, as shown in Fig. 7, but the orbit control vector and the sun vector described in the inertial frame were not. Using the TRIAD method, the attitude of the satellite with the smallest difference between the solar panel direction vector and the sun vector was calculated, while

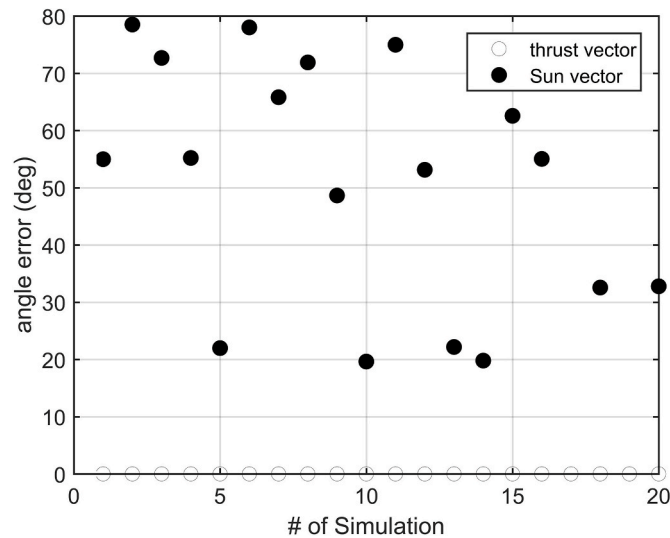


Fig. 12. Angle differences (○) between the real thrust direction and the desired orbit control direction, and the angle differences (●) between the solar panel direction and the Sun direction. The error in the orbit control is zero, but the Sun direction is not zero because the main purpose of attitude estimation for orbit controls is to match the orbit control direction vector and the thrust vector.

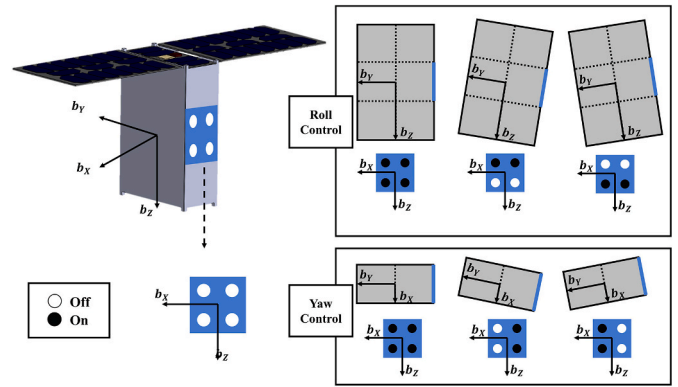


Fig. 13. Conceptual image of thrust modulation algorithm.

the thrust direction vector was matched with the orbit control vector. Therefore, the attitude calculated by the TRIAD method is the attitude in which the thrust direction is oriented toward the orbit control direction, and the solar panel is toward the Sun to the extent possible during orbit control. The attitude is calculated on the ground station and transmitted to the nanosats for the maneuvers.

#### 4.2. Attitude maintenance for orbit controls

Because the attitude cannot be controlled using the reaction wheel while generating the thrust due to the disturbance torque from thrust misalignment, the four thrust nozzles, with their on and off, is used to maintain the orbit control direction [26]. The thrust modulation algorithm is developed to maintain the control direction while the thrust module operates. So, the algorithm only activates during generating thrust to maintain the attitude of nanosat. The thrust module of the nanosat consists of four nozzles pointing to the same direction. The differences in the thrust magnitude between the nozzles and structural factors can produce a torque that changes the attitude of the nanosat while the orbit controls are in operation. The thrust modulation algorithm generates torque by the on and off control of each nozzle to reduce the angular velocity and errors in the orbit control direction. As shown in Fig. 13, the algorithm determines the activation of each nozzle to maintain the desired control direction.

To verify the algorithm, we conducted numerical simulations. The algorithm checks for the misalignment every 1 s and determines the on and off nozzles when the thrust direction error exceeds  $0.5^\circ$  or the rate exceeds  $0.3^\circ/\text{sec}$ . The moment of inertia of nanosat in the simulation was set as  $I_{xx} = 0.127 \text{ kgm}^2$ ,  $I_{yy} = 0.159 \text{ kgm}^2$ ,  $I_{zz} = 0.108 \text{ kgm}^2$  and off-diagonal terms were zeros. The error of the thrust magnitude of each nozzle was 10% ( $1\sigma$ ), and the center of mass was assumed to have an error of 1 cm ( $1\sigma$ ) from the geometric center of the nanosat in each axis. The initial control direction error was  $10^\circ$  ( $3\sigma$ ) and the angular velocity error was  $0.1^\circ$  ( $1\sigma$ ) in the roll and yaw axes. As shown in Fig. 7, the thrust module can generate torque in the roll and yaw axes because all nozzles are on the same plane. The algorithm can compensate for the torque caused by an imbalance in the thrust magnitude between each nozzle to ensure that the nanosat can maintain the orbit control direction for 100 s. Fig. 14 (a) shows that the initial control direction error was over  $3.5^\circ$ , but it decreased and remained within  $1^\circ$  after 20 s owing to the thrust modulation algorithm. Fig. 14 (b) shows the total magnitude generated by the thrust module, and Fig. 14 (c) shows the thrust magnitude of each nozzle. The thrust magnitudes of each nozzle are slightly different because the magnitude errors in each nozzle are different. When four nozzles were turned on, the magnitude was almost 0.1 N. The magnitude varied according to the on and off state of the nozzles. Through the thrust modulation algorithm, the direction of the thrust can be maintained within  $1^\circ$ , which is the requirement; thus, even if there is a difference in the thrust magnitude per nozzle, orbit control

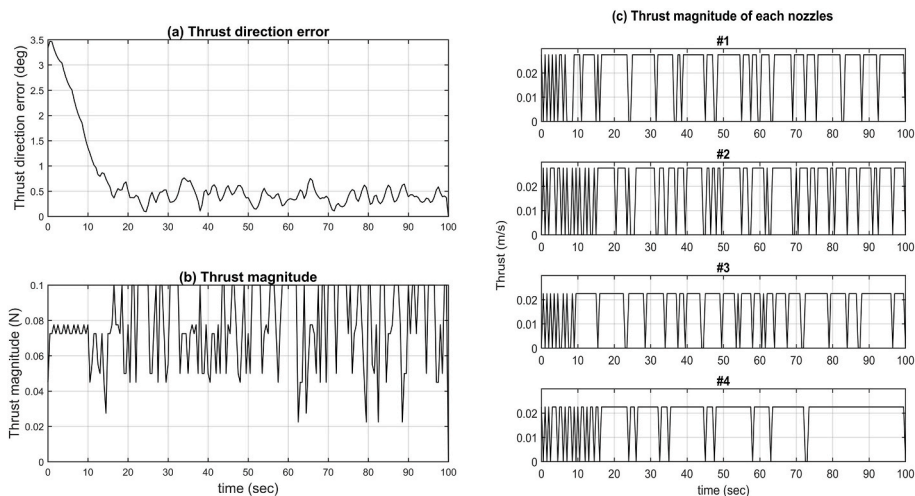


Fig. 14. Simulation results pertaining to thrust-modulation algorithm. The worst case represents the case wherein thrust magnitudes of the two top nozzles equal 27.5 mN, while those of the other two nozzles equal 22.5 mN. The angle error between the real thrust and desired orbit control direction is within 1°. The magnitude of total thrust varies depending on whether each nozzle is operational and differs for each nozzle.

Table 3  
Simulation setting of the dynamic model and parameters for orbit controls.

Contents		Specifications	
Dynamic model	Gravity model	JGM-3 30 by 30	
	Third body perturbation	Sun, Moon, Jupiter	
	Air drag model	MSISE90	
	Solar radiation pressure	Spherical model	
Parameters for orbit controls	Drag area	0.045 m <sup>2</sup>	
	Mass	10 kg	
	Thrust magnitude	25 mN per nozzle	
	Thrust module operation time	Along-track formation phase	– 30 s
		Cross-track formation phase	– 100 s
Total ΔV	50 m/s		
ΔV errors	ΔV magnitude	– 10% (1σ)	
	ΔV direction	– 13° (3σ)	
Orbit determination error	Position	– 15 m (1σ)	
	Velocity	– 0.03 m/s (1σ)	
Command interval	drift recovery	– 5 days	
	station keeping	– 5 days	
	initial configuration	– 3 days	
	reconfiguration	– 5 days	

can be conducted. Unfortunately, the thrust magnitude of each nozzle is unknown at the ground station during the control operation. Therefore, maintaining the thrust direction by means of a feedback control based on the attitude determination result using the thrust modulation algorithm embedded in the nanosat is necessary. The resulting thrust direction error is calculated using the thrust modulation algorithm and included in the telemetry received from the ground station.

5. Numerical simulations

The presented design of the formation flying system for the SNIPE mission was validated using numerical simulations. The General Mission Analysis Tool (GMAT) [27], a proven mission design tool, was used as a propagator, and the force model is presented in Table 3. Parameters for the orbit controls were set in consideration of the 6U-size nanosat. As the thrust magnitude of each nozzle was 25 mN, that generated by four nozzles was 100 mN. But the total thrust magnitude was 90 mN in the simulation because it was reduced by 10% because of thrust modulation algorithm. The maximum operating time of the thrust module was 30 s and 100 s in the along-track and cross-track formations, respectively.

Considering the power, the thrust module can be operated for 100 s. However, in the along-track formation phase, the maximum operating time is limited to 30 s to reduce the error by splitting the orbit controls. To simulate a finite burn, the time domain was discretized in 1-s intervals during simulations. The time interval between orbit control commands was 5 days for the along-track formation, 3 days for the initial configuration, and 5 days for the reconfiguration. The desired along-track formation duration was set to 75 ± 10 days. The magnitude error of ΔV was 10% (1σ), and the direction error of ΔV was 13° (3σ), which comprised of attitude determination and control error (10°, 3σ), and structural error (3°, 3σ). The orbit determination error in the position and velocity in each axis of inertial frame were 15 m (1σ) and 0.03 m/s (1σ), respectively. We could determine the ejecting direction of the nanosat from a launch vehicle individually; thus, the nanosats were set such that they are ejected from a single launch vehicle at 10 s time interval in a proper direction to drift away at equal distance intervals. The mission orbit was set to a sun-synchronous orbit with the perigee and apogee altitudes of the launch vehicle assumed to be 400 km and 600 km, respectively, and the longitude of the ascending node was 11 h. In the simulation, to confirm the cases of nanosats with various relative

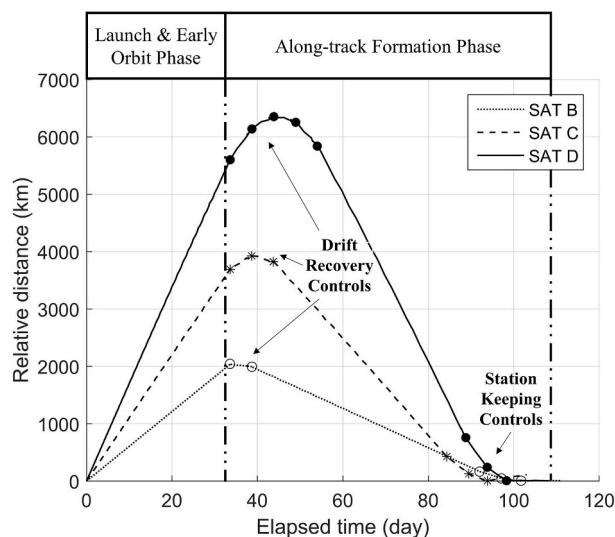


Fig. 15. Relative distances of each nanosats with respect to SAT A. The relative distance between the nanosats were modulated by the multiple finite burns.

distances, the reference nanosat was denoted by SAT A, which was the leading nanosat on the orbital plane among the four nanosats.

5.1. Drift recovery control for the along-track formation

The drift recovery control was used to gather the four nanosats to reduce the size of the along-track formation to observe various intervals of temporal data. The controls decreased the relative distances between the nanosats that have expanded in the LEOP. Fig. 15 shows the simulation results of the along-track formation. This shows that the distances of SAT B, SAT C, and SAT D increased from SAT A after being ejected from a launch vehicle during the initialization, stabilization, and commissioning duration, expressed as the LEOP. In this phase, SAT A, B, C, and D were ejected at the ejection angles 0°, 40°, 55°, and 70°, respectively and relative to the along-track direction on the orbital plane of the launch vehicle. A 0° ejection angle implies that the nanosat is ejected in the along-track direction of the launch vehicle (i.e., the velocity direction of launch vehicle). When a nanosat is ejected in the radial or cross-track direction, collision with a launch vehicle is possible, so the ejection velocity should have an along-track component. The LEOP will be 30 days according to the concept of operations. The maximum relative distance exceeded 6000 km, and the distances between nanosats were about 2000 km at the end of the LEOP as shown in Fig. 15.

After commissioning the thrust module, the nanosats performed the drift recovery controls described in Section 3.1 to decrease the relative distance with respect to the reference nanosat SAT A. The control changed the drift rate to be closer to the reference nanosat for the along-track formation phase. The markers on the left side of the along-track formation phase in Fig. 15 represents the drift recovery controls. If the calculated control operation time, which is required to reduce the distance for the along-track formation phase, exceeded the maximum control operation time, drift recovery controls were repeated after 5 days. Therefore, SAT B conducted the drift recovery controls twice to get closer to SAT A. Similarly, SAT C and D conducted three and four times of the controls, respectively. During the along-track formation phase, SAT B, C, and D moved on the cross-track and along-track plane of SAT A as described in Fig. 16. The relative distance shown in Fig. 15 exceeds the along-track position shown in Fig. 16 because the relative distance also considered the radial position. They approached the origin where the reference nanosat was located. It was confirmed in the control operation time of drift recovery control in Table 4 that all control operation time, except the last control, is the maximum control operation time. The largest ΔV consumption case was with SAT D, and the

Table 4

Numerical results of the along-track formation. The maximum control operation time in one orbit control is set to 30 s.

Parameters		SAT B	SAT C	SAT D
Drift recovery control	# of finite burns	2 times	3 times	5 times
	Accumulated ΔV	0.3635 m/s	0.7835 m/s	1.3048 m/s
Station keeping control	Control operation times	30 + 10 s	30 + 30+27 s	30 + 30+30 + 30+25 s
	Control commands	3 times	3 times	3 times
Duration for along-track formation	Accumulated ΔV	0.1317 m/s	0.2880 m/s	0.5940 m/s
	Control operation times	5 + 5+5 s	12 + 12+8 s	22 + 22+22 s
		69.3358 days	66.4424 days	75.3891 days

amount of ΔV was 1.26 m/s, which is less than 3 m/s than that of the ΔV budget for drift recovery controls, as shown in Table 2.

5.2. Station keeping control for the along-track formation

The station keeping control described in Section 3.2 was to maintain the relative distance between the nanosats to prevent the size of the along-track formation from increasing again. If station keeping controls are not performed, the difference in drift rate will be maintained and the relative distance between the nanosats will decrease and then increase again. The controls made the drift rate of the nanosat the same as the drift rate of the reference nanosat, SAT A. The markers on the right side of the along-track formation phase in Fig. 15 represents the station keeping controls. The number of commands for station keeping controls was set to three times to reduce the error, thereby ensuring that the variation in the relative distance caused by the errors in the orbit control was reduced after finishing the along-track formation phase. Nanosats started the station keeping control before the relative distance became too small to perform multiple times. The relative distances of SAT B, SAT C, and SAT D from SAT A were 5, 122, and 14 km, respectively, 10 days after the last station keeping control. The control operation time was obtained by dividing the control time required to make the same drift rate by the remaining number of commands for the station keeping control. Thus, it was confirmed in Table 4 that the control operation time used for each control in each nanosat was similar. The ΔV consumption of each nanosat was less than 0.5 m/s, which meets the ΔV budget of station keeping controls in Table 2. The durations for the

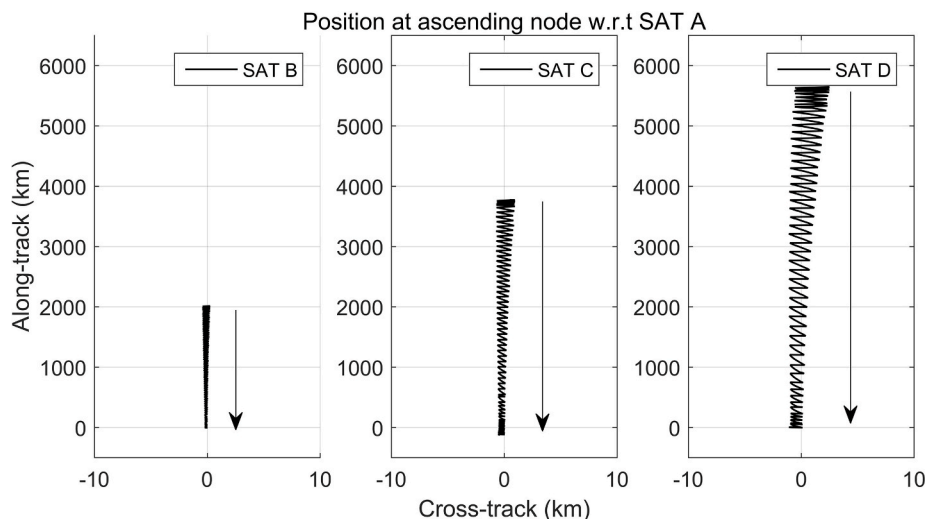
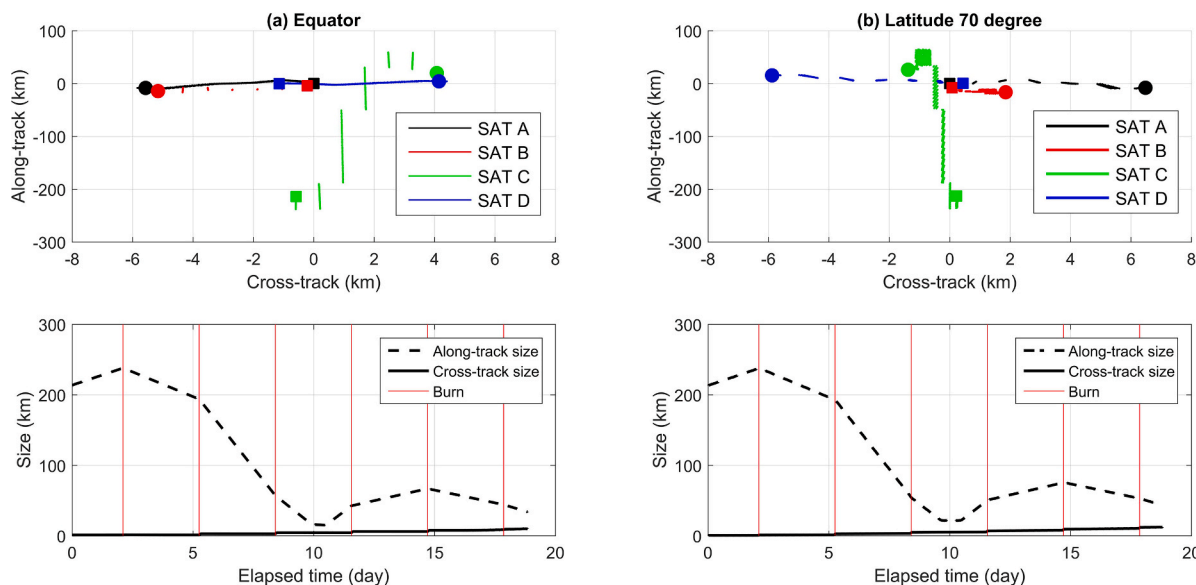


Fig. 16. Relative position of each nanosats with respect to SAT A at the ascending node in the along-track formation phase.



**Fig. 17.** Variation in position during the initial configuration at the equator (a) and at a latitude of 70° (b). The square and circle markers are the initial- and final position of each nanosat, respectively. The bottom two figures describe the time variation in the size of the cross-track formation. The size of the formation is the distance between the two farthest nanosats at the target latitudes in the along-track direction and cross-track direction.

along-track formation phase of each nanosat, time intervals between the initial control for drift recovery, and final control for station keeping, were over two months; consequently, the SNIPE mission could collect temporal data in this phase.

**5.3. Initial configuration control for the cross-track formation**

After all the nanosats have finished the station keeping control, the mission changed the shape of the formation from the along-track formation to the cross-track formation. The initial configuration control transposed the shape of the formation to observe the spatial data. SAT A and SAT D changed their inclination, whereas SAT B and SAT C changed their RAAN to alter the shape of formation from the along-track formation to the cross-track formation. Fig. 15 shows the result of the numerical simulation of the initial configuration control. The reference of the simulations was a propagated orbit of SAT A without orbit control from the end of the along-track formation phase. Fig. 17 also shows the changes in the position of the four nanosats over time on the cross-track and along-track plane of the reference at the equator and a latitude of 70°. SAT A, which increased its inclination, moved toward the right side with respect to the reference at the equator and the left side with respect to the reference at a latitude of 70° because of the variation in inclination and RAAN. SAT D moved in the opposite direction of SAT A because it decreased its inclination. Meanwhile, SAT B moved toward the left side with respect to the reference at the equator owing to a decreasing RAAN. It hardly moved at the latitude of 70° because the variation in RAAN barely affected the change in position at high latitudes. SAT C moved in the opposite direction of SAT B because it increased the RAAN.

**Table 5**

Numerical results of the simulation on the cross-track formation. With the same thrust performance, the four nanosats consume the same  $\Delta V$ .

Parameters	SAT A/B/C/D	
Initial configuration control	# of control commands	6 times
	Accumulated $\Delta V$	~6 m/s
Re-configuration control	Control operation times	100 s per command
	Control commands	18 times
	Accumulated $\Delta V$	~18 m/s
Duration for cross-track formation	Control operation times	100 s per command
		90 days

In Fig. 17, the four nanosats were placed as the square markers at the initial position of the simulation, which is the same as the relative position at the end of the along-track formation phase. The blue square marker indicates that SAT D is located with a relative distance of more than 70 km in the along-track direction, 10 days after all nanosats have finished the station keeping control. Nevertheless, through the along-track correction control that reduced the along-track direction position to maintain the shape of the cross-track formation in the initial configuration control, deformation of the formation in the along-track direction was maintained under 50 km. The circle markers in Fig. 17 indicate the position of the nanosats at the end of the initial configuration control phase. The shape of the formation changed from the along-track formation to the cross-track formation, and the size of the formation was longer than 10 km at the equator and a latitude of 70°. Each nanosat controlled its orbit every three days and a total of 6 times. The bottom two plots in Fig. 17 describe the time variation of the size of the cross-track and along-track formation sizes to increase and decrease, respectively. As shown in Table 5, all nanosats activated their thrust module for 100 s in every orbit control and consumed nearly 5.4 m/s of accumulated,  $\Delta V$  which is less than the 12 m/s,  $\Delta V$  budget for the initial configuration. Consequently, the initial configuration controls constructed the sizes of the cross-track formation to 10.0 and 12.3 km at the equator and at a latitude of 70°, respectively. Consequently, the formation can have a shape for observing the spatial differences.

**5.4. Reconfiguration control for the cross-track formation**

The reconfiguration control increased the size of the cross-track formation to gather various scales of spatial data in three months. After converting to the cross-track formation, the nanosats should extend the size of the formation using the reconfiguration controls. To increase the size, all nanosats changed their inclination. SAT A and SAT C increased their inclinations, while SAT B and D decreased their inclinations to extend the cross-track formation. The size of the formation expanded at a latitude of 70° because of the increase in the difference between the inclinations of the nanosats. Furthermore, the size at the equator also expanded because of the increase in the difference between time variations of RAAN by J2 perturbation, caused by the change in inclinations. All nanosats generated thrust for 100 s in each control

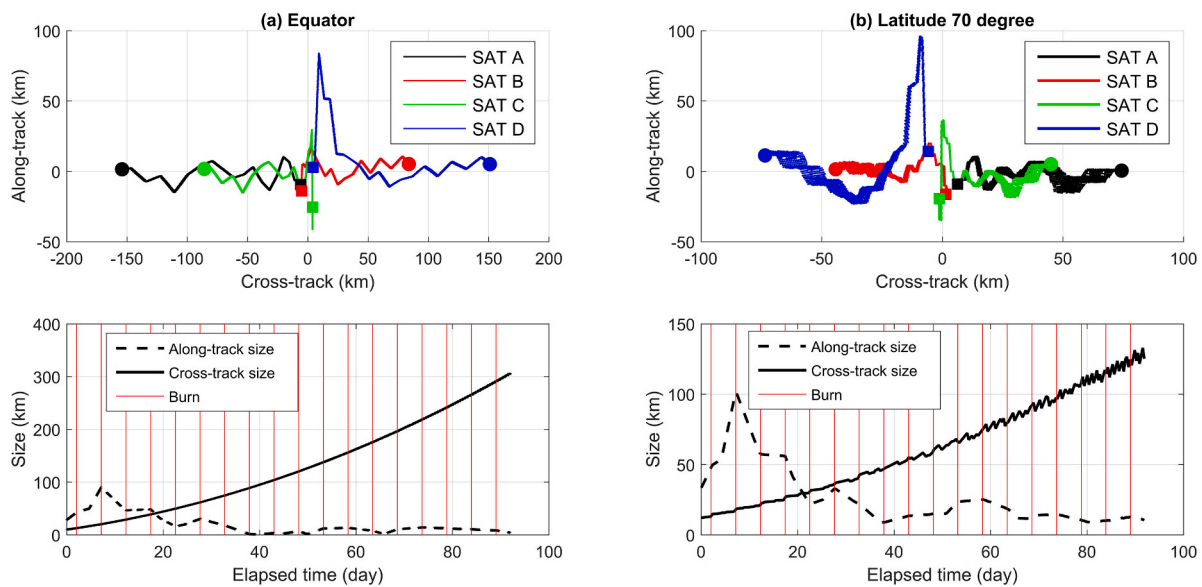


**Fig. 18.** Top two figures describe the variation in position during the cross-track formation for 3 months at the equator (a) and latitude 70° (b). Square and circle markers are the initial and final position of each nanosat, respectively. The bottom two figures describe the time variation in the size of the cross-track formation. The size of the formation is the distance between the two farthest nanosats at the target latitudes in the along-track direction and cross-track direction.

command, and the time interval between the commands was set to every 5 days. The simulation was performed for a case in which the control was repeated 18 times for three months. Fig. 18 shows the time variation of the nanosat positions on the cross-track and along-track plane of a reference. Nanosats were placed at the points of the circle markers at the start of the reconfiguration control and moved to the square markers. The state vector of reference was calculated by the propagation of the uncontrolled SAT A at the end of the along-track phase, which is the same as the reference in the simulation for the initial configuration control. The size of the formation in the cross-track direction changed up to 100 km at the equator and a latitude of 70°.

The bottom two figures in Fig. 18 show that the rate of the size of the cross-track formation became faster with respect to time because of the difference in inclination that increased. The cross-track size is the relative distance between the rightmost and leftmost nanosat. In this simulation, the size of the cross-track formation was the relative distance between SAT A and SAT D. As presented in Table 5, each nanosat activated the thrust module for 100 s in every orbit control command and consumed approximately 18 m/s of the accumulated  $\Delta V$  for 3 months, which was less than the  $\Delta V$  budget for the reconfiguration for 3 months (23 m/s). The size in the along-track direction was maintained within 20 km on average. The requirement for the size of the formation in the cross-track direction from the scientific objectives is more than 100 km at the target latitudes after 3 months. The size of the cross-track formation expanded from 10 km to 305 km at the equator, and from 12 km to 125 km at a latitude of 70° for 3 months.

## 6. Conclusions

This paper presents the design of a nanosat formation flying system and validation of the design for the SNIPE mission. The formations should observe the temporal and spatial differences of physical phenomena in the geomagnetic field. For these scientific objectives, the along-track and cross-track formations have been developed. The four nanosats that will perform the SNIPE mission planned to be ejected from a single launch vehicle and drifted apart during the LEOP. After the nanosats are ready to control their orbit, they decrease the relative distances during the along-track formation phase. The shape of the formation was transformed from the along-track to cross-track formation, and the size was extended by orbit control. To operate the two

types of formations, four types of orbit controls, namely, drift recovery, station keeping, initial configuration, and reconfiguration control, were derived. The orbit control methods were devised considering the J2 perturbation. The drift rate modulation was introduced to operate the along-track formation, and changes in the inclination and RAAN were considered during the cross-track formation. Orbit control scenarios were validated using numerical simulations that considered the constraints to implement the intended environment. The simulations reflected the limitation in terms of the time interval between the orbital information epoch and orbit control epoch, the inability to control the attitude during orbit control, constraints on power stability, and characteristics of the thrust module. The along-track formation could collect temporal data from 5000 km to less than tens of kilometers during ~70 days. Repeated maneuvers for the initial configuration switched the shape of the formation from along-track to cross-track formation. Switching the shape of the formation took 18 days. Then, periodic maneuvers for the reconfiguration extended the size of cross-track formation from 10 km to more than 100 km for 90 days to meet the scientific mission objective. The total accumulated  $\Delta V$  for each nanosat was below the  $\Delta V$  budget of 50 m/s, which comprises of the drift recovery, station keeping, initial configuration, reconfiguration control, and 20% margin. In the event where no uncertainties and constraints exist, an ideal environment,  $\Delta V$  could be calculated using a simple inverse matrix. However, the desired orbit control cannot be achieved under the constraints and uncertainties by the solution for the ideal environment. Unfortunately, redundancy does not exist, and recovery is impossible when the desired orbit control is not preformed due to hardware malfunction. To guarantee the robustness of the design and control method, simulations were performed for about 20 different cases, and it was confirmed that two types of formation flying operations were possible in all cases. If the thrust module cannot be used owing to power constraints or the thrust-direction error exceeds 10° because the thrust modulation algorithm malfunctions or the attitude control is executed abnormally, the nanosats do not perform orbit control and await the next orbit-control command. If the accuracy of orbital information is improved by using inter-satellite link or by increasing the frequency of communication between nanosats and the ground, more sophisticated formations can be operated. For the SNIPE mission, the result of this study can be implemented in formation flying dynamics software to integrate in the software of the ground station and perform the operation test to prepare the

acquisition phase.

### Funding sources

This work was supported by major research funding from Korea Astronomy and Space Science Institute (KASI).

### Declaration of competing interest

The authors declare that they have no known competing financial interests or personal relationships that could have appeared to influence the work reported in this paper.

### References

- [1] J. Hwang, H. Kim, J. Park, J. Lee, Limitations of electromagnetic ion cyclotron wave observations in low earth orbit, *J. Astron. Sp. Sci.* 35 (2018) 31–37, <https://doi.org/10.5140/JASS.2017.35.1.31>.
- [2] S. Kang, Y. Song, S. Park, Nanosat formation flying design for SNIPE Mission, *J. Astron. Sp. Sci.* 37 (2020) 51–60, <https://doi.org/10.5140/JASS.2020.37.1.51>.
- [3] R.M. Millan, R. von Steiger, M. Ariel, S. Bartalev, M. Borgeaud, S. Campagnola, J. C. Castillo-Rogez, R. Fléron, V. Gass, A. Gregorio, D.M. Klumpar, B. Lal, M. Macdonald, J.U. Park, V. Sambasiva Rao, K. Schilling, G. Stephens, A.M. Title, J. Wu, Small satellites for space science: a COSPAR scientific roadmap, *Adv. Space Res.* 64 (2019) 1466–1517, <https://doi.org/10.1016/j.asr.2019.07.035>.
- [4] D. Selva, D. Krejci, A survey and assessment of the capabilities of Cubesats for Earth observation, *Acta Astronaut.* 74 (2012) 50–68, <https://doi.org/10.1016/j.actaastro.2011.12.014>.
- [5] M.A.C. Silva, D.C. Guerrieri, A. Cervone, E. Gill, A review of MEMS micropropulsion technologies for CubeSats and PocketQubes, *Acta Astronaut.* 143 (2018) 234–243, <https://doi.org/10.1016/j.actaastro.2017.11.049>.
- [6] K. Lemmer, Propulsion for CubeSats, *Acta Astronaut.* 134 (2017) 231–243, <https://doi.org/10.1016/j.actaastro.2017.01.048>.
- [7] P. Muri, J. McNair, A survey of communication sub-systems for intersatellite linked systems and cubesat missions, *J. Commun.* 7 (2012) 290–308, <https://doi.org/10.4304/jcm.7.4.290-308>.
- [8] R. Radhakrishnan, W.W. Edmonson, F. Afghah, R.M. Rodriguez-Osorio, F. Pinto, S. C. Burleigh, Survey of inter-satellite communication for small satellite systems: physical layer to network layer view, *IEEE Comm. Surv. Tutor.* 18 (2016) 2442–2473, <https://doi.org/10.1109/COMST.2016.2564990>.
- [9] Di Mauro, M. Lawn, R. Bevilacqua, Survey on guidance navigation and control requirements for spacecraft formation-flying missions, *J. Guid. Contr. Dynam.* 41 (2018) 581–602, <https://doi.org/10.2514/1.G002868>.
- [10] S.J. Chung, S. Bandyopadhyay, R. Foust, G.P. Subramanian, F.Y. Hadaegh, Review of formation flying and constellation missions using nanosatellites, *J. Spacecraft Rockets* 53 (2016) 567–578, <https://doi.org/10.2514/1.A33291>.
- [11] N.G. Orr, J.K. Eyer, B.P. Larouche, R.E. Zee, Precision formation flight: the CanX-4 and CanX-5 dual nanosatellite mission, 21st Annual AIAA/USU Conference on Small Satellites (2007).
- [12] J.-P. Park, S.-Y. Park, Y.B. Song, G.N. Kim, K. Lee, H.J. Oh, J.-C. Yim, E.J. Lee, S.-H. Hwang, S.W. Kim, K.Y. Choi, D.S. Lee, S.H. Kwon, M.-S. Kim, S.-W. Yeo, T.-H. Kim, S.-H. Lee, K.B. Lee, J.-W. Seo, W.-H. Cho, J. Lee, J.-H. Park, Y.W. Kim, S. J. Kang, J. Hwang, S.H. Lee, J.-H. Yang, S. Jin, CubeSat development for CANYVAL-X mission, 14th International Conferences on Space Operations, SpaceOps (2016).
- [13] L. Alminde, M. Bisgaard, I.A. Portillo, T.A. Gornland, D. Smith, GOMX-4: Demonstrating the Building Blocks of Constellations, 2017, pp. 1–5.
- [14] C.W.T. Roscoe, J.J. Westphal, E. Moseleh, Overview and GNC design of the CubeSat proximity operations demonstration (CPOD) mission, *Acta Astronaut.* 153 (2018) 410–421, <https://doi.org/10.1016/j.actaastro.2018.03.033>.
- [15] G.-N. Kim, S.-Y. Park, D.-E. Kang, J. Son, T. Lee, S. Jeon, N. Kim, Y.-K. Park, Development of CubeSats for CANYVAL-C mission in formation flying, APISAT 2019 asia pacific, in: *Asia Pacific International Symposium on Aerospace Technology*, 2019, pp. 813–824.
- [16] N.H. Roth, B. Risi, C.C. Grant, R.E. Zee, Flight results from the CanX-4 and CanX-5 formation flying mission, 4S Symp (2016) 1–15, <https://doi.org/10.1016/j.jcrsgr.2014.02.053>.
- [17] R. Walker, GOMX-4 – the twin European mission for IOD purposes, in: 32nd Annual AIAA/USU Conference on Small Satellites, 2018, pp. 813–824.
- [18] D. Ran, X. Chen, A.K. Misra, B. Xiao, Relative position coordinated control for spacecraft formation flying with communication delays, *Acta Astronaut.* 137 (2017) 302–311, <https://doi.org/10.1016/j.actaastro.2017.04.011>.
- [19] D. Ivanov, M. Kushniruk, M. Ovchinnikov, Study of satellite formation flying control using differential lift and drag, *Acta Astronaut.* 152 (2018) 88–100, <https://doi.org/10.1016/j.actaastro.2018.07.047>.
- [20] D. Lee, Nonlinear disturbance observer-based robust control for spacecraft formation flying, *Aero. Sci. Technol.* 76 (2018) 82–90, <https://doi.org/10.1016/j.ast.2018.01.027>.
- [21] D.M. Vallado, A. David, *Fundamentals of Astrodynamics and Applications*, second ed., McGraw-Hill Companies, Inc., New York, 1997.
- [22] J. Newman, Drift recovery and station keeping results for the historic CanX-4/CanX-5 formation flying mission, in: 29th Annual AIAA/USU Conference on Small Satellites, 2014.
- [23] G. Fasano Opromolla, G. Rufino, M. Grassi, Design of relative trajectories for in orbit proximity operations, *Acta Astronaut.* 145 (2018) 342–356, <https://doi.org/10.1016/j.actaastro.2018.01.062>.
- [24] R.H. Battin, *An Introduction to the Mathematics and Methods of Astrodynamics*, AIAA Education Series, New York, 1999.
- [25] H.D. Black, A passive system for determining the attitude of a satellite, *AIAA J.* 2 (1964) 1350–1351, <https://doi.org/10.2514/3.2555>.
- [26] S. Lee, *Development of Attitude Determination and Control and Thrust Modulation Algorithms for Formation Flying of the SNIPE Nano-Satellite*, Yonsei, 2019.
- [27] S.P. Hughes, R.H. Qureshi, D.S. Cooley, J.J.K. Parker, T.G. Grubb, Verification and validation of the general mission analysis tool (GMAT), *AIAA/AAS Astrodyn. Spec. Conf.* 2014 (2014), <https://doi.org/10.2514/6.2014-4151>.